Simple retinal imaging system using a MEMS scanning mirror

doi: 10.1117/1.OE.57.9.095101

Optical Engineering

OpticalEngineering.SPIEDigitalLibrary.org

Simple retinal imaging system using a MEMS scanning mirror

Neelam Kaushik
Takashi Sasaki
Toru Nakazawa
Kazuhiro Hane

SPIE.

Neelam Kaushik, Takashi Sasaki, Toru Nakazawa, Kazuhiro Hane, "Simple retinal imaging system using a MEMS scanning mirror," *Opt. Eng.* **57**(9), 095101 (2018), doi: 10.1117/1.OE.57.9.095101.

Simple retinal imaging system using a MEMS scanning mirror

Neelam Kaushik,[a,*] Takashi Sasaki,[a] Toru Nakazawa,[b] and Kazuhiro Hane[a]
[a]Tohoku University, Graduate School of Engineering, Sendai, Japan
[b]Tohoku University, Graduate School of Medicine, Sendai, Japan

Abstract. We have fabricated a simple and compact scanning laser optical system using microelectromechanical system (MEMS) scanner that can be incorporated into portable health monitoring devices. The two-dimensional (2-D) MEMS scanner used in this system is much smaller and light in weight compared to galvanometer scanners and polygon scanners used in the commercially available ophthalmic devices. MEMS scanners have many advantages and also limitations compared to galvanometer and polygon scanners. An easy to use and compact device is more useful for rapid alignment for measurement and data acquisition. Sensitivity of the system was quantified by measuring signal-to-noise ratio (SNR) for both high and low reflectivity materials. SNR was 10 for the high reflectance materials and about 4 for low reflectance materials, which is sufficient for biological imaging. Distortion generated using large scanning angle of 2-D MEMS scanner was corrected in real time by custom made LabVIEW program. Ocular safety is important to consider when using a laser for ophthalmic devices. We calculated the maximum permissible beam power for thermal damage and photochemical damage considering the specification of our system such as visual angle and wavelength of the laser beam. The measured laser intensity in the front of model eye was 6 μW, which is much smaller than the maximum permissible beam power recommended by the American National Standards Institute. [DOI: 10.1117/1.OE.57.9.095101]

Keywords: optical scanners; micromirror; retinal imaging system; scanning laser ophalmoscope.

Paper 180874 received Jun. 18, 2018; accepted for publication Aug. 28, 2018; published online Sep. 12, 2018.

1 Introduction

More than 30% of human population suffer from vision related diseases/defects. Some of these defects develop with time. Images of retina/fundus are important for diagnosis. The discovery of confocal scanning laser ophthalmoscope (SLO) in 1987 by Webb et al. provided a new method for retinal imaging.[1] SLO is a noninvasive, noncontact optical imaging technique that has become a basic method to diagnose and monitor retinal diseases.[2] The confocal nature of SLO minimizes the effect of scattered light from out-of-focus tissue and helps to get high contrast, high resolution images from retina. SLO system has been used for various clinical applications for the detection of retinal diseases such as detection of glaucoma, age-related degeneration of macula, etc.[3–5] But many eye diseases remain undetected until irreversible vision loss happens due to limited access to specialized equipment, and the high cost of retinal imaging devices makes the wide spread screening for eye diseases impractical. Regular screening of eye is necessary for detection, avoidance, and treatment of eye diseases.[6] Eye monitoring tool should have adequate sensitivity to detect retinal defects, easy to use, and portable enough to be carried outside of hospitals or clinics.

However, most commercial SLO systems are bulky and table mounted, which limits their application for deployment of screening. Many modern SLO use galvanometer scanners and rotating polygonal scanners for beam steering on the sample.[7–9] Both types of scanners have their own advantages and drawbacks. Galvanometer-controlled scanners are large in size and usually used for slow scanning. Galvanometer scanners are slow in operation due to their size, inertia, and they require to slowdown and reverse direction. Polygon scanners allow fast scanning with adjustable speed, but the angular range is limited by number of facets, effectively fixing the field of view (FOV). Another disadvantage of polygon scanner is that the rotation axis is far from the mirror face that leads to the variation of axial path length during one scan.

To facilitate smaller and portable SLO instruments, microelectromechanical system (MEMS) mirrors or scanners can be used for high speed beam steering. MEMS scanners are made by using semiconductor technology and are available in different range of sizes varying from 0.5 to 5 mm with moderate optical angles. MEMS scanners are more adaptable and cost effective. Two-dimensional (2-D) MEMS scanners that scan in two axes are alternatively used in place of large galvanometer scanners for various optical coherence tomography systems in endoscopic applications.[10–13] However, there are very few reports of MEMS scanner being used in SLO system; in this work, we report on a simple MEMS scanner-based SLO system. MEMS scanners are preferred as they are cost effective, allow miniaturization, in addition to better performance at resonant high-frequency actuation. Another advantage of using MEMS scanners is low power consumption per scan axis. In addition to many advantages, MEMS scanners do have some limitations that are mainly related to the operational environment and materials used for the fabrication of mirror. For example, one of the potential failure mechanisms of MEMS mirror

*Address all correspondence to: Neelam Kaushik, E-mail: neelam@hane.mech.tohoku.ac.jp

0091-3286/2018/$25.00

can be material fatigue that can slightly change resonant frequency of MEMS scanners. Material fatigue is most likely to occur at the torsion hinge attaching the mirror to the frame. This can be improved by using metallic glass as a material for torsion hinge because it is free from granular structure and have much higher elastic strain limit.[14] The purpose of fabricating MEMS-based SLO is to implement the optical system for personal health care monitoring such as portable retinal imaging system.

2 Methods

2.1 *Design and Experimental Setup*

The basic design of the fabricated system is shown in Fig. 1(a). A 633-nm He–Ne laser was used for illuminating the retina of model eye. The laser beam was collimated by an 11-mm focal length, 6.6-mm diameter collimating lens. The collimated beam had a 2.1-mm ($1/e^2$) diameter, and it is reflected from a MEMS scanner and focused on the retina by relay optics. Achromatic doublet lenses (L1 and L2) with focal length of 50 mm were used to minimize chromatic aberration. Beam magnification was kept unity.

The 2-D-MEMS scanner (model no. ESS240A, NIPPON SIGNAL) used in the system is shown in Fig. 1(b), and it is square shaped with dimensions of ~4 mm × 4 mm. MEMS scanner had 2170 and 410 Hz resonant frequencies in X and Y axes. The optical angle of the scanner as mentioned in data sheet is ±8.5 deg but considering the safe limit and stable operation the maximum scan angle of ±7.0 deg was used during the experiment. The MEMS scanner was controlled by a custom made driving circuit, and it was operated in an open loop. The driving frequencies of X- and Y-axes during measurements were 1.79 kHz and 10 Hz, respectively.

The reflected light from the retina was detected by a photomultiplier tube (PMT) (H10721-20), Hamamatsu, Japan) through a pinhole. For the confocal pinhole, a multimode fiber with a diameter equals to 1.6 times the airy disc diameter was employed. The focal length of the collection lens (L3) was 50 mm and the core diameter of the multimode fiber was 50 μm. The detected signal was low pass filtered with a cut off frequency of 1 MHz, which is approximately half of the sampling frequency in order to avoid aliasing artifacts in the image. A 2-D image of the retina was obtained by changing the angle of MEMS scanner. Different scan areas were used for the experiments. Scan area was varied by changing the frequency of fast axis and amplitude of slow axis. The detected signals were acquired using AI-1204Z-PCI card (12-bit) (Contec Co., Ltd. Japan). Custom software developed using LabVIEW was used for real-time display of the images obtained by the setup. An image correction program was also developed using LabVIEW that was implemented for correcting distortion in the obtained images. To characterize the imaging performance of the system, we used two model eyes. One was fabricated in the lab and another was custom made by the company. For the fabricated model eye, an uncoated N-BK7 planoconvex-lens with a focal length of 35 mm and curvature radius of 7.7 mm was used that acted as human cornea. The custom made model eye was made up of N-BK7 glass, and it consists of patterns very similar to human eye such as optic disc and blood vessels on a diffusing surface (refractive index = 1.52, cornea = 1.38).

2.2 *Optical Design and Performance*

The maximum FOV of our system was 14.0 deg according to calculation considering magnification factor and peak-to-

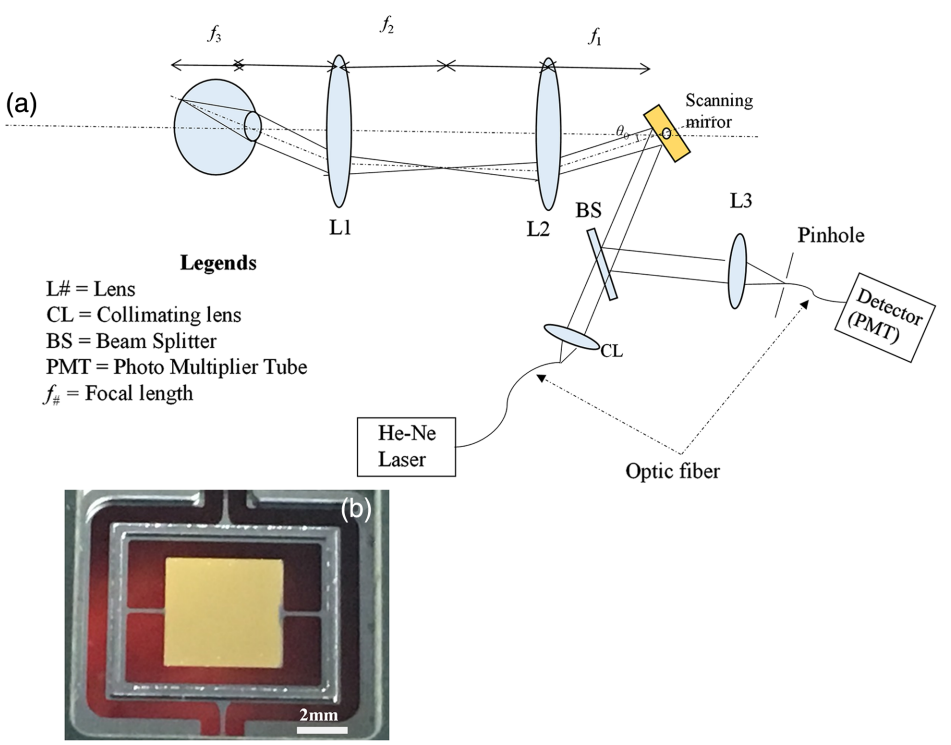

Fig. 1 (a) Basic design of fabricated optical system and (b) photograph of the 2-D MEMS scanner used in the system.

peak maximum optical scan angle of scanner used for the measurement. The imaging speed was 20 frames per second (fps) with 180 lines per frame. The optical system design was made by using an optical design software ZEMAX (Optima Research, United Kingdom) at a design wavelength of 633 nm. The optical design was optimized by minimizing spot sizes covering the FOV at the intermediate plane and along the retina of model eye. Nearly diffraction limited performance was obtained in Zemax for 14-deg FOV. The eye model was created based on the parameters similar to human eye. Spot diagrams, off-axis point-spread function (PSF) plot, and modulation transfer function (MTF) plots were obtained and are shown in Fig. 2. Spot diameters for the system illumination on the retina spanning a 14-deg FOV are shown in Fig. 2(a). The system was diffraction limited at 7 μm (airy disk radius). Airy disk is shown by black circle on spot diagrams. PSF of the designed system at the retina is shown in Fig. 2(b), which is narrow, which means the transition at the edge from white to black is not wide and imaging performance is good according to calculations. The box containing the PSF was 32×32 μm^2. The Strehl ratio was 0.882. MTF graph shows the contrast (modulus of OTF) in the image as a function of the resolution in the image (spatial frequency in cycles per mm) at nominal focus. The black curve represents the theoretical best result, i.e., diffraction limited MTF and blue curve represents the MTF of actual system covering 14-deg FOV. The calculated MTF curve shows resolution performance is close to theoretical results.

The measured incident power on the model eye was 6 μW, which is within the American National Standard for Safe Use of Lasers (ANSI) standards for safe retinal exposure at 633 nm. We calculated the maximum permissible exposures for ocular safety by considering the specification of our system that are explained later in results and discussion section.

3 Results and Discussion

To demonstrate the capabilities of our optical system for its application in portable and wearable devices, we checked some important functions such as resolution, signal-to-noise ratio (SNR), image stabilization, and image correction. Prevention of ocular exposures during retinal imaging is important factor that should be considered while designing an optical system using lasers. We calculated the maximum permissible beam powers for thermal and photochemical exposure using our optical system. Detailed results from the experiments are explained consecutively in this section.

3.1 *Resolution*

The resolution of the system was measured with a 1951 USAF resolution test target as the model retina. The resolution test target has a series of horizontal and vertical lines that are used to determine the resolution of an imaging system. A set of six elements is in one group, and there is a total of 10 groups in the resolution chart. Figures 3(a) and 3(d) show the images of big and small line pattern of the target taken by an optical microscope. Big line pattern represents group 3 element 4 and small line pair patterns are from group 4. Reflectance images obtained by scanning the target are shown in Figs. 3(b) and 3(e). Cross section from the areas

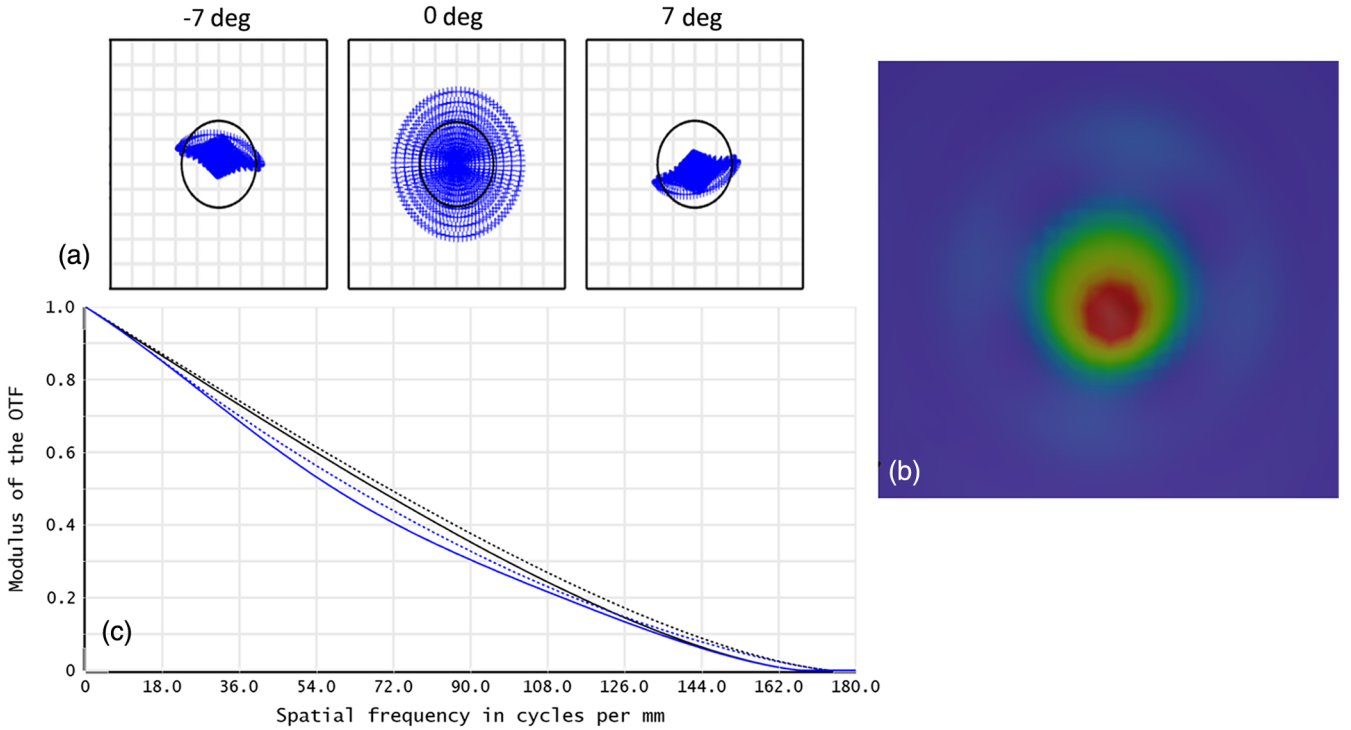

Fig. 2 (a) Spot diagram for the fabricated system illumination on the retina for 14-deg FOV. The system is nearly diffraction limited at 7 μm (the airy disk radii). (b) PSF of the designed system at the retina for one of the outermost configuration. The box containing the PSF was 32×32 μm^2. The Strehl ratio was 0.882 (c) MTF of the system for configurations spanning 14-deg FOV on the retina of model eye. The black curve represents the diffraction limited MTF and blue curve represents the MTF of three configuration spanning a 14-FOV on the retina.

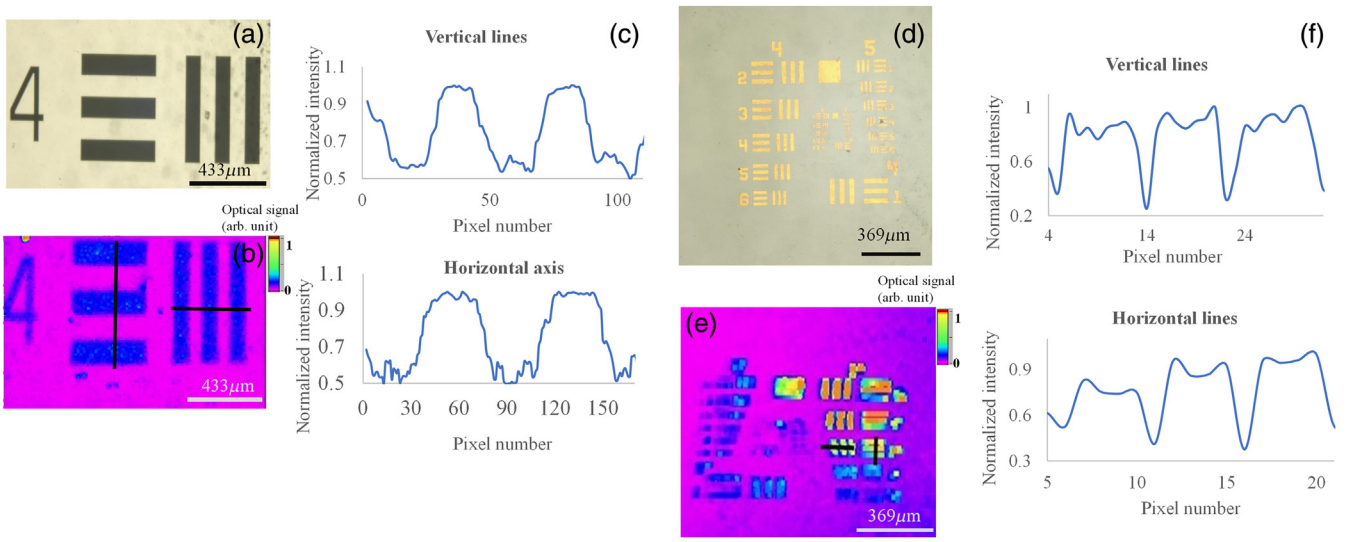

Fig. 3 Lateral resolution of optical system: (a) optical image of group 3 element 4 of a 1951-USAF resolution target, (b) reflectance image of the patterns shown in Fig. 3(a), cross section from horizontal and vertical lines of (b) is shown in (c). Optical images of group 4 and group 5 are shown in (d). (e) is the reflectance image of (d). Cross section from horizontal and vertical lines of 3(e) is shown in (f). Three different peaks are resolved giving a resolution of 44.2 μm.

indicated by black lines in Figs. 3(b) and 3(e) is shown in Figs. 3(c) and 3(f), respectively. Slight distortion in the image Fig. 3(e) can be observed and that results from the use of MEMS mirror that rotates about separate axes and these can be corrected by using a correction table if needed. The smallest line pairs that could be resolved by our system were group 4 element 4, which corresponds to a lateral resolution of 44.2 μm. For comparison, the size of main retinal arteries is about 200 μm and the smallest retinal capillaries are between 10 and 20 μm, so our system has enough resolution for imaging retinal arteries and optics disc for the detection of eye-related disorders. We also estimated the total resolvable spots for our system with respect to scanning area of MEMS scanner. The number of resolvable spots describes the relationship between FOV and resolution of any scanning system. If the system has a small number of resolvable spots over a wide field, then the small features may not be resolved. The resolvable spots can be estimated by scanning mirror diameter d_m and the optical scan angle $\pm\Theta_m$. The diffraction angle for the focused Gaussian beam in terms of mirror diameter can be written as

$$\Theta_{\text{diff}} = \tan^{-1}[2.45 * (\lambda_0/\pi d_m)],$$

where λ_0 is the center wavelength used in the system.

According to Rayleigh criterion of resolution, two spots can be resolved if the angle between the two peak intensities is equal to twice of the diffraction angle at $1/e^2$ intensity. The number of resolvable spots for the scanning system can be calculated by ratio of total scanning angle and twice of diffraction angle:

$$\text{Total resolvable spots} = 2\Theta_m/2\Theta_{\text{diff}}.$$

For our setup, we used a MEMS scanner with 4 mm in diameter and $\pm$7.0-deg optical angle for all the measurements. So according to the theoretical calculation, resolvable spots for our system are 990. The measured spot size on the retina of the model eye was about 8.4 μm ($1/e^2$ diameter), and the scan length on the model retina was 8.5 mm, so we calculated the number of resolvable spot by dividing the total scan length by spot diameter.

The calculated resolvable spots are 1011, which are very close to the theoretical value. Optical design calculation by using Zemax (MTF curves) also showed the resolution performance is close to theoretical calculation. But in real experimental conditions, the resolution of our system is not exactly the same as the diffraction limited value, it is slightly lower than the calculated value. The reason for lower resolution than the theoretical calculated resolution is that in Zemax calculations, MTF curves of lenses explain only the first link of the imaging chain and do not take into account those that follow, such as scanner, sensor, etc., so the total resolution of the system is dependent on other components as they also have transfer functions.

3.2 *Signal-to-Noise Ratio*

As the reflectance signal from the biological tissues is not very high in the visible range wavelength, it is important to check the SNR. According to Webb and Hughes, the SNR should be expressed as the ratio of total number of signal photons received by the detector per pixel to the standard deviation of the photon fluctuation number per pixel,[15] but real SNR is difficult to estimate experimentally from the pixelated image, as it is not easy to measure the signal and noise photons exactly within a certain pixilation time.

For the SLO systems, the image is acquired using an analog-to-digital converter that digitalizes the analog output of photo detector. Although, theoretically, the total amount of noise can be predicted but, experimentally, estimation of exact amount of noise in the system is challenging. Considering these facts, the signal-to-noise performance of the system was checked by using material with different reflectance from high to very low reflectance. Figures 4(a)–4(c) show

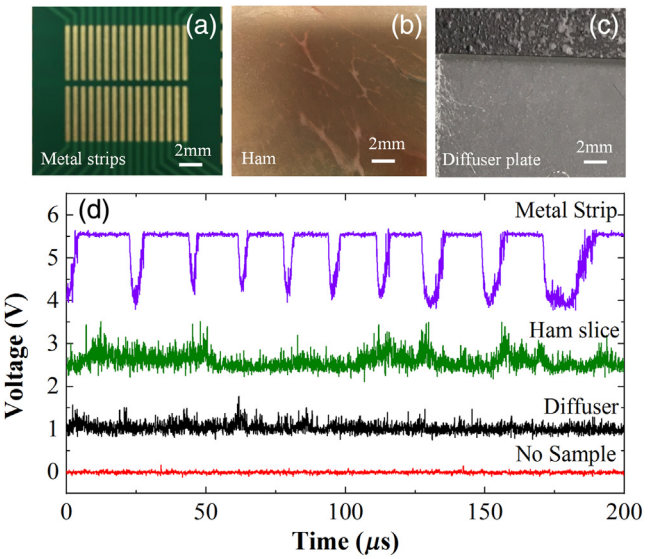

Fig. 4 (a) Photograph of metal strip sample, (b) and (c) are photographs of ham and diffuser sample used for the measurement, (d) response of PMT at control voltage of 0.7 V for three different samples.

the images of the samples used for measuring SNR of the system.

For high reflectance material, we used a metal strip sample and for the low reflectance sample a diffuser plate was used. To check the sensitivity of the system for biological tissues we used a ham slice. Response of PMT is shown in Fig. 4(d). Vertical axis shows change in voltage with respect to different samples and horizontal axis represents the time in seconds. The control voltage for the photo multiplier tube (PMT) was 0.7 V. As expected, the SNR for metal strip sample was high compared to other materials. The noise level in the system is very low. The reflectance signal for the diffuser is also low. The reflectance signal for ham sample is higher than the diffuser. The peaks in the response of ham slice represent the tissues with high reflectance. It is same for the metal sample. The voltage is high for metal strip and it becomes very low for the space in between the two metal strips. The SNR was about 4 for the low reflectance materials. The SNR for the biological samples was measured at different gain control voltage of the PMT ranging from 0.5 to 0.9 V. The SNR increased by increasing the gain control voltage of the PMT. The system shows enough sensitivity to observe biological tissues.

3.3 *Imaging and Image Stabilization*

We developed custom software in LabVIEW (National Instruments, Austin, Texas) for image acquisition and background subtraction. The images were corrected in real time for background noise removal. Figure 5(a) shows the reflectance signal from a custom made model eye. In Fig. 5(a), the light colored vein-like structure represents thin blood vessels and bright contrasted pattern is similar to optic disc-like pattern on the retina of model eye. For biological sample, we used a thin ham slice and an enucleated swine eye. Figure 5(b) is the photograph of ham sample.

Reflectance signal was obtained from two different scan areas marked by square in dotted lines on Fig. 5(b). Bright colored spots in Figs. 5(c) and 5(d) represent the tissues with high reflectance and some vein-like patterns are also visible similar to white lines in photograph of ham sample. The light contrast line patterns and base represents the tissues with low reflectance. Figure 5(e) is the photograph of enucleated swine eye that was used for the imaging and reflectance signal obtained by scanning swine eye is shown in Fig. 5(f). The bright oval part in the image represents the optic disc of swine eye and dark lines near are the blood vessels. The reflectance signal from biological samples is not so high, but imaging was possible even for low reflectance signals. These results clearly show that this system can be used for retinal imaging.

3.4 *Image Correction*

Resonant scanner resonates at their natural frequencies, which are in order of several kilohertz. However, resonant scanners have some drawbacks. One major problem is that the velocity of scanned laser beam projected on the sample changes in a cosinusoidal manner, i.e., it is slow at the edges and speed is maximum in the middle of the scanned field. Thus, when image data are acquired from such resonant scanning system with a frame grabber at constant pixel rate, the images appear stretched at the edges.[16] In our setup, 2-D image is obtained by progressively scanning in bidirectional manner, i.e., odd lines from left-to-right and even lines from right-to-left that yields acquisition rates of 20 fps. The speed of forward scan and backward scan is not symmetrical, and it is restricted by acceleration of fast scan, which makes line shift distortion.

Several solutions have been proposed to solve this problem. The simplest one is to use limited image width of the scan area, where the scan speed is almost linear.[16] But this will also limit the size of scanned image. Another method to improve image distortion caused by mismatch of scan speed in fast and slow axis is to separate forward scan and backward scan during image acquisition. We made a very simple program in the LabVIEW for the separation of forward scan and backward scan. Images can be acquired in the real time. The flowchart of the software for image construction and correction program is shown in Fig. 6. For large scan area, where distortion was observed, a correction table was added to the obtained image data. We used the same sample with metal strip to acquire images by an ordinary program and with a correction program. In the ordinary program, images from both the scans, i.e., forward scan and backward scans were added together, whereas in correction program images were separated for each scan type.

Figure 7(a) is the optical image of sample with metal strips and Fig. 7(b) shows the reflectance image of the same sample. The scan area is small so there is no visible distortion in the image. Figures 7(c) and 7(d) are the reflectance images of the sample shown in Fig. 7(a) with large scanned area. Scan area is biggest in Fig. 7(d) and distortion can be seen at the edges of both images [Figs. 7(c) and 7(d)].

Figure 7(d) shows the image of sample acquired by ordinary normal one frame scan program. In this image, we can clearly observe stretching of image at the edges and some line shift distortion. The center part of the image is without any distortion. Separated scans that are forward scan and backward scan only are shown in Figs. 7(e) and 7(f), respectively. In the separated scan images, the stretching of the image at the edge looks corrected. There are some white

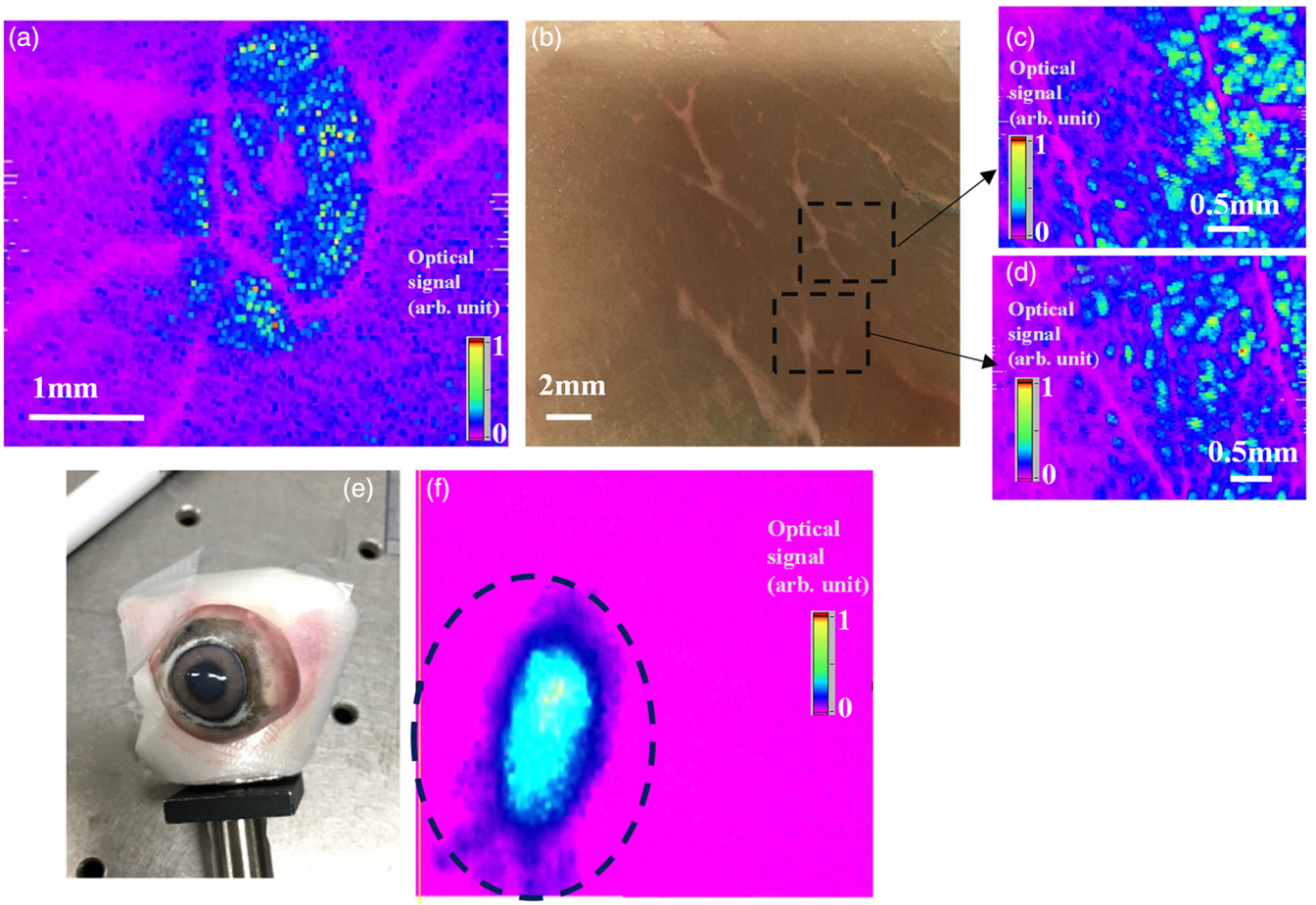

Fig. 5 (a) Reflectance signal from model eye showing the blood vessels and optic disc-like structures, (b) photograph of ham sample, (c) and (d) are reflectance signal from ham, (e) photograph of enucleated swine eye, and (f) reflectance signal from swine eye.

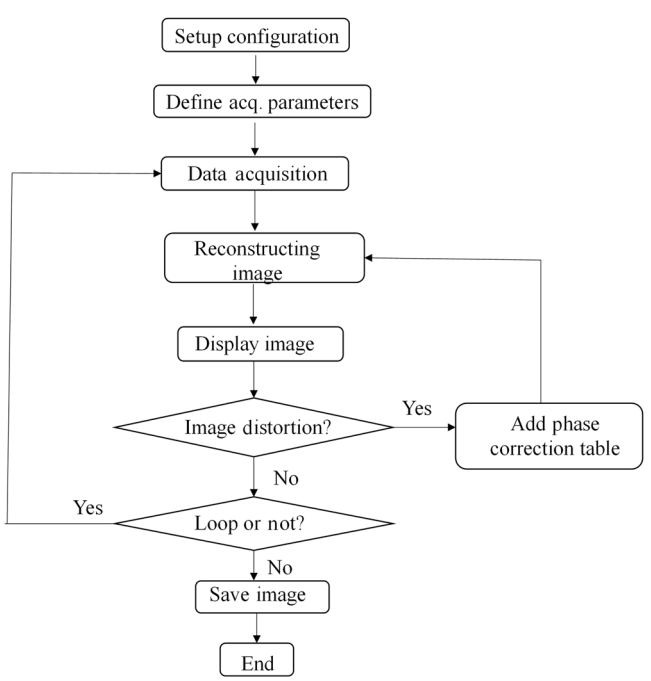

Fig. 6 Flowchart for image construction and correction program.

lines in the center part of the separated images, and those are due to reduction of number of pixel in separated scans. The pixel number reduced by half in forward and backward scans.

Some bending in the image is due to 2-D scan of two-axis mirror, i.e., the optical path lengths are little different when the light is directed at different points on a flat surface.[17] The use of a simple software program helps to avoid the need for any hardware and simplifies the instrument design.

3.5 *Safety Issues*

The literature about SLO often reports about the details of laser power used, which is usually below the safely limits prescribed by the ANSI laser safety standards. These regulations explain about the maximum permissible exposure and maximum laser power over a certain pupil area on the cornea that should be used for safety of patients.[18] There may be no perfect method to estimate the potential hazard from the retinal exposure of an SLO. We should first check the static beam, i.e., no scanning power in front of the eye. In our case, the laser power of static beam was 6 μW, which is quite low. We calculated the maximum beam power for our setup considering the visual angle for an exposure of 300 s (5 min). We used a continuous wave laser with 633-nm wavelength. For the thermal limit, the

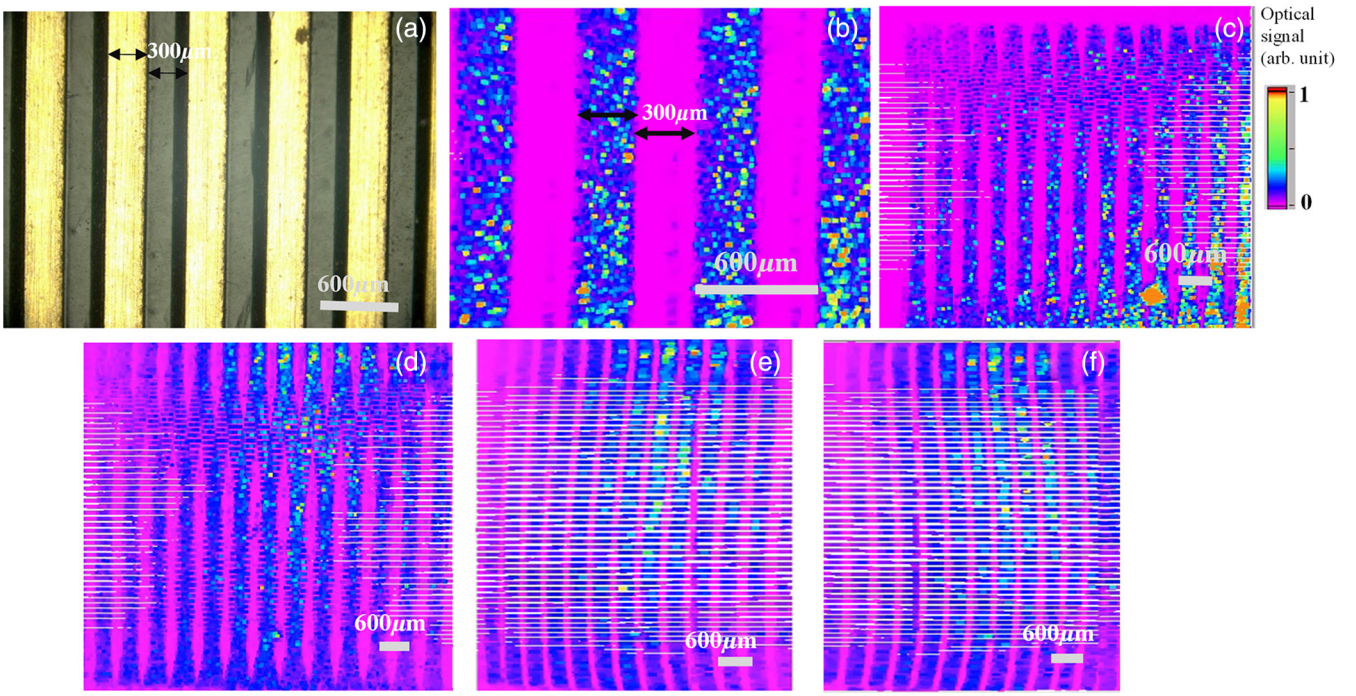

Fig. 7 (a) Optical image of metal strip sample. (b) Reflectance image of small scan area, (c) large scan area, (d) large scan area showing distortion at the edges due to bidirectional scan, (e) separated forward scan, and (f) separated backward scan.

maximum permissible $\mathrm{MP}\Phi_{\mathrm{B}}$ (in watts) beam power was calculated using[18]

$$\mathrm{MP}\Phi_{B,\mathrm{CW,th}} = 1.41 \times 10^{-6}\, C_T P_{300}^{-1} \alpha_F^2,$$

where C_T is function of wavelength and it is 1 for λ (400 to 700 nm). P is pupil function which is also defined by wavelength and time.[19] The exposure time was 300 s which is realistic duration for most clinical and experimental situations. The visual angle (α_F) was 122.5 mrad and the calculated value for $\mathrm{MP}\Phi_{\mathrm{B,CW,th}}$ is 3.8 mW.

The photochemical limits in watts was calculated as[19]

$$\mathrm{MP}\Phi_{\mathrm{B,CW,ph}} = 2.36 \times 10^{-8}\, C_B \alpha_F^2,$$

where C_B is the function of wavelength and for λ (400 to 700 nm) it is $10^{0.020(\lambda\text{-}450)}$.[19] The calculated value for $\mathrm{MP}\Phi_{\mathrm{B,CW,ph}}$ is 1.6 W. The measured laser intensity in front of model eye is much lower than the calculated maximum permissible beam power limits for thermal and photochemical damage. Therefore, it is safe to use our fabricated system for imaging of human eye.

4 Conclusions

A simple and compact SLO with high signal to noise was fabricated using a 2-D MEMS scanner. The images from model eye and swine eye were successfully obtained. One of the main advantages of using 2-D MEMS scanner is that it can shrink system size, which is important to make portable imaging system and other is fast scanning. These advantages can enable this system to be applied as an easy to use screening tool for retinal imaging. The fabricated system has enough resolution for the observation of main retinal arteries and optic disc for early diagnosis of eye disorders such as glaucoma. Image distortion was corrected using a simple program in real time without adding any unnecessary hardware. The results are promising and will be used for the development of portable health monitoring devices.

References

1. R. H. Webb, G. W. Hughes, and F. C. Delori, "Confocal scanning laser ophthalmoscope," *Appl. Opt.* **26**(8), 1492–1499 (1987).
2. R. H. Webb and G. W. Hughes, "Scanning laser ophthalmoscope," *IEEE Trans. Biomed. Eng.* **BME-28**(7), 488–492 (1981).
3. W. N. Wykes, A. A. E. Pyott, and Y. G. M. Ferguson, "Detection of diabetic retinopathy by scanning laser ophthalmoscopy," *Eye* **8**(4), 437–439 (1994).
4. A. Manivannan et al., "Clinical investigation of an infrared digital scanning laser ophthalmoscope," *Br. J. Ophthalmol.* **78**(2), 84–90 (1994).
5. S. Wolf et al., "Retinal hemodynamics using scanning laser ophthalmoscopy and hemorheology in chronic open-angle glaucoma," *Ophthalmology* **100**(10), 1561–1566 (1993).
6. S. Rowe, C. H. MacLean, and P. G. Shekelle, "Preventing visual loss from chronic eye disease in primary care: scientific review," *JAMA* **291**(12), 1487–1495 (2004).
7. P. Saggau, "New methods and uses for fast optical scanning," *Curr. Opin. Neurobiol.* **16**(5), 543–550 (2006).
8. J. J. Hunter et al., "Characterizing image quality in a scanning laser ophthalmoscope with differing pinholes and induced scattered light," *J. Opt. Soc. Am. A* **24**(5), 1284–1295 (2007).
9. S. A. Burns et al., "Contrast improvement of confocal retinal imaging by use of phase-correcting plates," *Opt. Lett.* **27**(6), 400–402 (2002).
10. J. T. W. Yeow et al., "Micro machined 2-D scanner for 3-D optical coherence tomography," *Sens. Actuators A Phys.* **117**(2), 331–340 (2005).
11. W. Jung et al., "Three-dimensional endoscopic optical coherence tomography by use of a two-axis micro electromechanical scanning mirror," *Appl. Phys. Lett.* **88**, 163901 (2006).
12. K. H. Kim et al., "Two-axis magnetically-driven MEMS scanning catheter for endoscopic high-speed optical coherence tomography," *Opt. Express* **15**(26), 18130–18140 (2007).
13. D. Wang et al., "Endoscopic swept source optical coherence tomography based on a two-axis micro electromechanical system mirror," *J. Biomed. Opt.* **18**(8), 086005 (2013).
14. J. W. Lee et al., "Micro mirror with large-tilting angle using Fe-based metallic glass," *Opt. Lett.* **36**(17), 3464–3466 (2011).

15. R. H. Webb and G. W. Hughes, "Detectors for scanning video imagers," *Appl. Opt.* **32**, 6227–6235 (1993).
16. N. Callamaras and I. Parker, "Construction of a confocal microscope for real-time x-y and x-z imaging," *Cell Calcium* **26**, 271–279 (1999).
17. M. Hafez, T. Sidler, and R. P. Salathe, "Study of the beam path distortion profiles generated by a two-axis tilt single-mirror laser scanner," *Opt. Eng.* **42**(4), 1048–1057 (2003).
18. ANSI, "American National Standard for safe use of lasers (ANSI 136.1)," ANSI 136.1-2000, The Laser Institute of America (2000).
19. F. C. Delori, R. H. Webb, and D. H. Sliney, "Maximum permissible exposures for ocular safety (ANSI 2000) with emphasis on ophthalmic devices," *J. Opt. Soc. Am. A* **24**(5), 1250–1265 (2007).

Neelam Kaushik received her PhD in material science and engineering from Tohoku University, Sendai, Japan, in 2010. She worked as research associate from 2010 to 2016 in WPI-AIMR, Tohoku University. She has been working as an assistant professor with the Department of Fine Mechanics, Tohoku University since 2017. Her research interest includes development of health monitoring systems using MEMS devices and new materials for MEMS application.

Takashi Sasaki received his MS and PhD degrees in mechanical engineering from Tohoku University, Sendai, Japan, in 2009 and 2012, respectively. Since 2012, he has been an assistant professor with the Graduate school of Engineering, Tohoku University, where he is currently engaged in research and development of microelectromechanical systems for sensor applications.

Toru Nakazawa received his PhD in ophthalmology in 2002. He spent the following three years at Massachusetts Eye and Ear Infirmary as the research fellow. He has been a professor and chairman of Department of Ophthalmology at Tohoku University since 2011. His research interest includes development of clinical therapy by using the results of basic research. He has published more than 254 articles in board reviewed international journals.

Kazuhiro Hane received his MS and PhD degrees from Nagoya University, Japan, in 1980 and 1983, respectively. From 1983 to 1994, he was with the Department of Electrical Engineering, Nagoya University. From 1985 to 1986, he was a visiting researcher with the National Research Council of Canada. Since 1994, he has been a professor with the Graduate School of Engineering, Tohoku University, Japan. His research interest includes development of optical microsensors and optical microelectromechanical systems.